

# The Geometry of Most Probable Trajectories in Noise-Driven Dynamical Systems

John C. Neu,<sup>1</sup> Akhil Ghanta,<sup>2</sup> and Stephen Teitsworth<sup>2</sup>

<sup>1</sup>*Duke University, Department of Biomedical Engineering, Box 90281 Durham, NC 27708-0281*

<sup>2</sup>*Duke University, Department of Physics, Box 90305 Durham, NC 27708-0305*

(Dated: September 25, 2018)

This paper presents a heuristic derivation of a geometric minimum action method that can be used to determine most-probable transition paths in noise-driven dynamical systems. Particular attention is focused on systems that violate detailed balance, and the role of the stochastic vorticity tensor is emphasized. The general method is explored through a detailed study of a two-dimensional quadratic shear flow which exhibits bifurcating most-probable transition pathways.

Keywords: transition path, geometric stochastic action, fluctuation loops

## I. INTRODUCTION

In the final chapter of Feynman and Hibbs' classic text on path integrals [1], the scattering of a fast particle from nuclei in a slab of material is examined in order to answer the question: what is the most probable path of the particle from emitter to detector? The relative probabilities of noise sequences which produce paths with the required endpoints can be represented as a functional of the paths themselves. The variational characterization of the most probable path is closely analogous to least action paths in mechanics, or geodesic paths in geometry (a special case of the former). Independently, a rigorous theory of most probable paths in stochastic dynamical systems was developed by Wentzell and Freidlin [2, 3], and subsequently elaborated and explored by many others, see e.g. [4]. Additionally, a similar formalism for treating large noise-induced deviations has been applied more recently to spatially-extended hydrodynamic models [5, 6].

In applications to concrete problems, physicists [7, 8] often employ the Legendre transformation to convert the Lagrangian formulation of most probable paths into an equivalent Hamiltonian formulation. Here we retain the Lagrangian formulation, to see very directly some geometric aspects of most probable paths (see Sec. II). A geometrical characterization of most probable paths was recently introduced by Heymann and Vanden-Eijnden [9–11], and we recapitulate aspects of their treatment in the language of classical mechanics at the level of a typical physics graduate course. A chief advantage is that there are very clear expressions of some common insights: in the small noise limit, almost all paths with fixed endpoints closely follow the most probable path in an almost deterministic manner. Furthermore, the speed along the most probable path is the deterministic speed. As the noise decreases, the transit time between endpoints remains fixed, but the expected time between successful transits becomes exponentially large.

In Section III, we discuss the geometric meaning of *detailed balance*, a fundamental notion from statistical physics. The traditional meaning of detailed balance, or its breaking, is framed in terms of the probability current in the Fokker-Planck equation: “fence off” a bounded re-

gion of state space with the impermeable boundary condition, and allow the probability density to relax to a steady state within that region. For a detailed balance system, the probability current vanishes identically, and there is a potential energy function so that the equilibrium probability density is proportional to a Boltzmann factor with this potential. If detailed balance is broken, the steady probability current is divergence-free, as it must be, but does *not* vanish identically [12, 13]. We review how this traditional characterization of detailed balance restricts the velocity field and noise tensor of the stochastic dynamics, so that the *stochastic vorticity tensor* vanishes. Furthermore, there is a connection to the geometry of most probable paths: in detailed balance systems, the “backward” path associated with an interchange of the starting and destination endpoints is the reversal of the original “forward” path. If detailed balance is broken, this reversibility is broken. In this case, the path from starting to destination point and then back again to the starting point forms a loop, and the sense of rotation around the loop is determined by the vorticity [14, 15].

## II. THE GEOMETRIC ACTION

We begin by reviewing the statistics of noise driven trajectories, in the spirit that was formulated many years ago by Feynman and Hibbs [1]. The state space is  $\mathbb{R}^N$ , and trajectories are curves  $\mathbf{x} = \mathbf{x}(t)$  in state space parametrized by time  $t$ . The  $\mathbf{x}(t)$  satisfy a Langevin equation

$$\dot{\mathbf{x}} - \mathbf{u}(\mathbf{x}) = \sqrt{\epsilon}\sigma\mathbf{w}(t). \quad (1)$$

Here,  $\mathbf{u}(\mathbf{x})$  is a given flow vector field on state space, the components of  $\mathbf{w}(t)$  are independent unit white noises, and  $\sigma$  is a noise tensor, assumed uniform and constant.  $\epsilon > 0$  is a gauge parameter, so we can formalize the small noise limit  $\epsilon > 0$ . The Langevin equation (1) with uniform and constant noise tensor  $\sigma$  is physically appropriate when the noise represents external forcing as a function of time, by degrees of freedom not included in  $\mathbf{x}$ .

The trajectories we consider are solutions of (1) which pass through two given points  $\mathbf{a}$  and  $\mathbf{b}$  of state space in succession. There is no restriction on the time of flight  $T$  from  $\mathbf{a}$  to  $\mathbf{b}$ . Due to autonomy, we can set the origin of time so  $\mathbf{x}(0) = \mathbf{a}$ . Then  $\mathbf{x}(T) = \mathbf{b}$ . The essential idea is that the relative probability of such a trajectory from  $\mathbf{a}$  to  $\mathbf{b}$  is the same as the relative probability of the white noise  $\mathbf{w}(t)$  in  $0 < t < T$  which produces it. The relative probability of a noise sequence  $\mathbf{w}(t)$  in  $0 < t < T$  is expressed formally as

$$e^{-\frac{1}{4} \int_0^T |\mathbf{w}(t)|^2 dt}. \quad (2)$$

For the intuition behind (2), model the sample space of white noises in  $0 < t < T$  by piecewise constant functions. Any one component of  $\mathbf{w}(t)$  is represented by  $w(t) \equiv w_j$  in  $(j-1)\Delta t < t < j\Delta t$ . Here, the time increment is  $\Delta t = \frac{T}{N}$  for some positive integer  $N$ . There are  $N$  time intervals of piecewise constant  $w(t)$  in  $0 < t < T$ . The constant values of  $w(t)$  in different time intervals are statistically independent, and the probability density of each  $w_j$  is proportional to the Gaussian

$$e^{-\frac{w_j^2}{2(\frac{2}{\Delta t})}} = e^{-\frac{1}{4} w_j^2 \Delta t}, \quad (3)$$

with mean square  $\frac{2}{\Delta t}$ . Due to the independence of the  $w_j$  for different  $j$ , the probability density in the  $\mathbb{R}^N$  of  $N$ -tuples  $(w_1, \dots, w_N)$  which characterize whole noise sequences in  $0 < t < T$  is the product of the Gaussians (3),

$$e^{-\frac{1}{4} (\sum_1^N w_j^2) \Delta t}. \quad (4)$$

We now see that the formal integral (2) is a shorthand reminder of this construction. The choice of mean square  $\frac{2}{\Delta t}$  for each  $w_j$  gives the correct behavior of the Brownian motion,

$$B(t) := \int_0^t w(t') dt'. \quad (5)$$

At  $t = n\Delta t$ , we have

$$\langle B^2(t) \rangle = n \left( \frac{2}{\Delta t} \right) (\Delta t)^2 = 2n\Delta t = 2t. \quad (6)$$

In this little review, we have presented (2) as the relative probability of noise sequences subject to no constraints. The noise sequences  $\mathbf{w}(t)$  which actually produce a trajectory with starting point  $\mathbf{a}$  and endpoint  $\mathbf{b}$  are in a restricted class - i.e., they must obey the boundary conditions, and we assume that the relative probabilities within this restricted class are still characterized by (2).

The relative probability (2) is converted into a functional of the trajectory  $\mathbf{x} = \mathbf{x}(t)$  in  $0 < t < T$  simply by “solving” the stochastic differential equation (1) for  $\mathbf{w}(t)$ ,

$$\mathbf{w}(t) = \frac{1}{\sqrt{\epsilon}} \sigma^{-1} (\dot{\mathbf{x}} - \mathbf{u}), \quad (7)$$

and substituting this  $\mathbf{w}(t)$  into (2). The relative probability is thereby expressed as

$$e^{-\frac{1}{\epsilon} S[\mathbf{x}(t)]}, \quad (8)$$

where  $S[\mathbf{x}(t)]$  is the *stochastic action functional*, given by

$$S[\mathbf{x}(t)] := \frac{1}{4} \int_0^T (\dot{\mathbf{x}} - \mathbf{u}) \cdot D^{-1} (\dot{\mathbf{x}} - \mathbf{u}) dt. \quad (9)$$

Here,

$$D := \sigma \sigma^T \quad (10)$$

is the *diffusion tensor* associated with the noise tensor  $\sigma$ . In this whole train of thought, we are assuming that  $\sigma$  is invertible [11].

The global minimizer  $\mathbf{x}(t)$  of the action (9) is called the *most probable trajectory*. The minimization of the action determines the *geometric curve*  $C$  that  $\mathbf{x}(t)$  traces out the path from  $\mathbf{a}$  to  $\mathbf{b}$ , and also the time sequence of positions along  $C$ . In particular, the flight time  $T$  is precisely determined by (21) below. The traditional analysis [8] begins with the Euler-Lagrange equation of the action (9), with  $T$  fixed. The Lagrangian is

$$L(\mathbf{x}, \mathbf{v} := \dot{\mathbf{x}}) := \frac{1}{4} (\mathbf{v} - \mathbf{u}) \cdot D^{-1} (\mathbf{v} - \mathbf{u}). \quad (11)$$

Due to autonomy, there is a conserved “energy”

$$h(\mathbf{x}, \mathbf{v}) = \mathbf{v} \cdot \nabla_{\mathbf{v}} L - L = \frac{1}{4} (\mathbf{v} \cdot D^{-1} \mathbf{v} - \mathbf{u} \cdot D^{-1} \mathbf{u}). \quad (12)$$

Some presentations carry out a Legendre transformation from Lagrangian to Hamiltonian dynamics [8, 16]. Here, we stay within the Lagrangian framework. Think of  $D^{-1}$  as the metric tensor of the  $\mathbb{R}^N$  in which  $\dot{\mathbf{x}}$  and  $\mathbf{u}$  live. The associated inner product is

$$\mathbf{f} \bullet \mathbf{g} := D^{-1} \mathbf{f} \cdot \mathbf{g}, \quad (13)$$

and the squared “length” of  $\mathbf{f}$  is

$$|\mathbf{f}|^2 := \mathbf{f} \bullet \mathbf{f}. \quad (14)$$

In geometric notation, the action (9) is

$$\begin{aligned} S &= \frac{1}{4} \int_0^T |\dot{\mathbf{x}} - \mathbf{u}|^2 dt \\ &= \frac{1}{4} \int_0^T (\dot{\mathbf{x}} \bullet \dot{\mathbf{x}} - 2\mathbf{u} \bullet \dot{\mathbf{x}} + \mathbf{u} \bullet \mathbf{u}) dt \\ &= \frac{1}{4} \int_0^T (|\dot{\mathbf{x}}|^2 - 2|\dot{\mathbf{x}}||\mathbf{u}| + |\mathbf{u}|^2) dt + \frac{1}{2} \int_0^T (|\mathbf{u}||\dot{\mathbf{x}}| - \mathbf{u} \bullet \dot{\mathbf{x}}) dt, \end{aligned}$$

or, finally,

$$S = \frac{1}{4} \int_0^T (|\dot{\mathbf{x}}| - |\mathbf{u}|)^2 dt + \frac{1}{2} \int_0^T (|\mathbf{u}||\dot{\mathbf{x}}| - \mathbf{u} \bullet \dot{\mathbf{x}}) dt. \quad (15)$$

The first integral on the right hand side achieves its minimum value of *zero* if the speed  $|\dot{\mathbf{x}}(t)|$  of the trajectory matches the speed  $|\mathbf{u}(\mathbf{x}(t))|$  of the deterministic flow,

$$|\dot{\mathbf{x}}(t)| = |\mathbf{u}(\mathbf{x}(t))|. \quad (16)$$

Given (16), the action (15) reduces to

$$S = \frac{1}{2} \int_0^T (|\mathbf{u}||\dot{\mathbf{x}}| - \mathbf{u} \bullet \dot{\mathbf{x}}) dt. \quad (17)$$

In (17), we recognize

$$\mathbf{dx} = \dot{\mathbf{x}} dt, \quad (18)$$

and

$$ds = |\mathbf{dx}| = |\dot{\mathbf{x}}| dt. \quad (19)$$

as increments of displacement and arclength in elapsed time  $dt$ , respectively. Hence, the action (9) reduces to a geometric line integral along the curve  $C$  connecting  $\mathbf{a}$  to  $\mathbf{b}$ ,

$$S = \frac{1}{2} \int_C (|\mathbf{u}| ds - \mathbf{u} \bullet \mathbf{dx}). \quad (20)$$

In summary, the most probable trajectory  $\mathbf{x}(t)$  from  $\mathbf{a}$  to  $\mathbf{b}$  proceeds with deterministic speed as in (16), and the geometric curve  $C$  traced out by  $\mathbf{x}(t)$  minimizes the line integral (20).

We acknowledge some collateral insights: since the speed along  $C$  is the deterministic speed, the time of flight from  $\mathbf{a}$  to  $\mathbf{b}$  is

$$T = \int_C \frac{ds}{|\mathbf{u}|}. \quad (21)$$

A further consequence of (16) is that the most probable trajectory lives on the null surface of the energy (12) in  $\mathbf{x}, \dot{\mathbf{x}}$  space. In geometric notation, (12) reads

$$h = \frac{1}{4} (|\dot{\mathbf{x}}|^2 - |\mathbf{u}|^2) \quad (22)$$

and (16) implies  $h = 0$ . In the important special case where the most probable paths connect *critical points*, we can deduce directly that  $h \equiv 0$  and hence  $|\dot{\mathbf{x}}| = |\mathbf{u}|$  because  $\dot{\mathbf{x}}$  and  $\mathbf{u}$  both vanish at critical points. But the null Hamiltonian character of most probable paths is more general. In the preceding argument, we have seen that the speed along the least action fluctuational path between *any* two endpoints equals the deterministic speed. Hence the null Hamiltonian character of most probable paths applies to any pair of endpoints, be they critical or not.

The propagation along  $C$  at deterministic speed seems deeply peculiar when we reflect that it is an asymptotic result of the small noise limit  $\epsilon \rightarrow 0$ . Notice that we can halve the noise amplitude, and half the noise still drives the *same* speed of propagation along  $C$ . Here is another

collateral insight: A change in  $\epsilon$  can be absorbed by scaling the diffusion tensor  $D$ . Look at the contribution to the time of flight  $T$  from a small segment  $\mathbf{dx}$  of  $C$ . The increment of arclength is

$$ds = \sqrt{D^{-1} \dot{\mathbf{x}} \cdot \dot{\mathbf{x}}} dt,$$

the speed is

$$|\mathbf{u}| = \sqrt{D^{-1} \mathbf{u} \cdot \mathbf{u}},$$

and it is clear that the scaling of  $D$  does not change the time increment  $dt = \frac{ds}{|\mathbf{u}|}$ .

A qualitative explanation might go like this: The noise induced sequence of kicks that drives the speed  $|\mathbf{u}|$  must have some “winning” combination of strength and unidirectionality, and it must last throughout the flight time  $T$ . As the noise amplitude goes to zero, the time duration of a “winning streak” ( $\mathbf{x}(t)$  goes from  $\mathbf{a}$  to  $\mathbf{b}$ ) remains near  $T$ , cf. (21), but the expected time *between* winning streaks becomes exponentially large.

### III. BROKEN DETAILED BALANCE AND THE GEOMETRY OF LEAST ACTION PATHS

We begin with some details behind the overview of detailed balance in the introduction. Let  $\rho(\mathbf{x}, t)$  be the ensemble probability density. The probability current generated by the stochastic dynamics (1) is

$$\mathbf{J} := \rho \mathbf{u} - D \nabla \rho. \quad (23)$$

Here,  $\mathbf{u}(\mathbf{x})$  is the velocity field of the stochastic differential equation (1), and  $D$  is the diffusion tensor (10). Take a bounded region  $\mathcal{R}$  of state space, and impose the impermeable boundary condition,  $\mathbf{J} \cdot \mathbf{n} = 0$  on  $\partial \mathcal{R}$ . Then the probability density in  $\mathcal{R}$  asymptotes to a time independent steady state  $\rho = \rho(\mathbf{x})$ . In a detailed balance system, the probability current is not only divergence-free, but vanishes identically, so

$$\rho \mathbf{u} = D \nabla \rho \quad (24)$$

throughout  $\mathcal{R}$ . It follows from (24) that

$$\nabla(\log \rho) = D^{-1} \mathbf{u} \quad (25)$$

or, equivalently, the *stochastic vorticity tensor*  $\Omega$ , with components

$$\Omega_{ij} := \partial_j (D^{-1} \mathbf{u})_i - \partial_i (D^{-1} \mathbf{u})_j, \quad (26)$$

vanishes.

To see the role of vorticity in the geometry of most probable paths, we write down the variational differential equation of the geometric action (20). Let  $\mathbf{x} = \mathbf{x}(s)$  be the parametric representation of a most probable path with respect to the arclength  $s$ . Then, the variational equation is

$$\frac{d}{ds} (|\mathbf{u}| D^{-1} \frac{d\mathbf{x}}{ds}) - \nabla |\mathbf{u}| = \Omega \frac{d\mathbf{x}}{ds}. \quad (27)$$

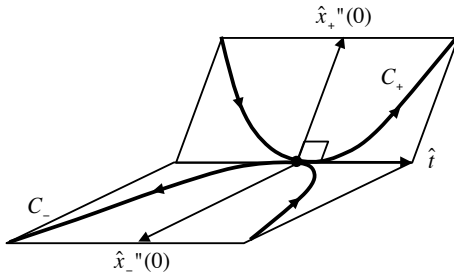


FIG. 1: Illustration of trajectories  $C_+$  and  $C_-$  which just touch at position  $\mathbf{X}$  with oppositely directed tangent vectors.

Evoking the close analogy to geometric optics [17], any curve traced out by a solution of (27) is called a *ray*. The LHS of (27) is invariant under orientation reversal ( $s \rightarrow -s$ ), but the RHS changes sign if the vorticity is nonzero. Hence, the forward and backward paths between two endpoints in a region of nonzero vorticity are generally not reversals of each other. The addition of forward and backward paths makes a closed loop, whose orientation is determined by the vorticity tensor.

A simple local analysis of rays informs the structure of forward plus backward loops whose endpoints are close to each other. Let  $C : \mathbf{x} = \mathbf{x}(s)$  be a curve parametrized by arclength  $s$ . Set the origin of arclength so as to mark a given point  $\mathbf{X}$  on  $C$ . In the Taylor series of  $\mathbf{x}(s)$  as  $s \rightarrow 0$ , we have

$$\mathbf{x}(s) = \mathbf{X} + \mathbf{x}'(0)s + \frac{1}{2}\mathbf{x}''(0)s^2 + O(s^3), \quad (28)$$

where the tangent  $\mathbf{x}'(0)$  at  $\mathbf{X}$  is a unit vector,  $|\mathbf{x}'(0)| = 1$  (since the expansion is with respect to arc length), and the second derivative is orthogonal to the tangent,  $\mathbf{x}'(0) \bullet \mathbf{x}''(0) = 0$ . If  $\mathbf{x}''(0) \neq 0$ , we see that  $C$  near  $\mathbf{X}$  is asymptotic to a parabola in the plane spanned by  $\mathbf{x}'(0)$  and  $\mathbf{x}''(0)$ . Now look at two particular rays  $C_+ : \mathbf{x}_+(s)$  and  $C_- : \mathbf{x}_-(s)$  which meet at  $\mathbf{X}$  at  $s = 0$ , with opposite and equal tangents,  $\hat{\mathbf{t}} := \mathbf{x}'_+(0) = -\mathbf{x}'_-(0)$ . From the ray equation (27), it follows that the vorticity induces a *difference* of second derivatives,

$$[\mathbf{x}''(0)] := \mathbf{x}''_+(0) - \mathbf{x}''_-(0) = \frac{2}{|\mathbf{u}|} D\Omega \hat{\mathbf{t}}. \quad (29)$$

To see this, we evaluate (27) at  $s = 0$  to obtain  $|\mathbf{u}|D^{-1}\mathbf{x}''(0) + (\mathbf{x}'(0) \cdot \nabla)|\mathbf{u}|D^{-1}\mathbf{x}'(0) - \nabla|\mathbf{u}| = \Omega\mathbf{x}'(0)$ . Note that the second and third terms on the LHS of this equation are invariant under reversal, ( $s \rightarrow -s$ ). Thus, taking differences evaluated along  $C_+$  and  $C_-$ , we can write  $|\mathbf{u}|D^{-1}[\mathbf{x}''(0)] = \Omega[\mathbf{x}'(0)] = 2\Omega\hat{\mathbf{t}}$ , from which (29) follows directly.

The antisymmetry of  $\Omega$  implies that  $[\mathbf{x}''(0)]$  is orthogonal to  $\hat{\mathbf{t}}$ , as it must be, since  $\mathbf{x}''_+(0)$  and  $\mathbf{x}''_-(0)$  are. For  $\Omega\hat{\mathbf{t}} \neq 0$ , we can visualize  $C_+$  and  $C_-$  near  $\mathbf{X}$  as two parabolas tangent to each other at  $\mathbf{X}$ , but bending in different planes,  $C_+$  in the plane of  $\hat{\mathbf{t}}$  and  $\mathbf{x}''_+(0)$ , and

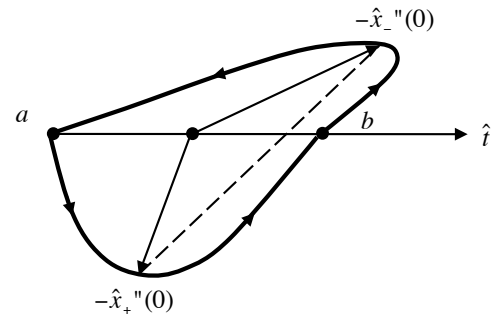


FIG. 2: Illustration of “forward” and “backward” loops for endpoints  $\mathbf{a}$  and  $\mathbf{b}$  in the neighborhood of  $\mathbf{X}$ , obtained by translating  $C_+$  in the  $-\mathbf{x}''_+(0)$  direction and  $C_-$  in the  $-\mathbf{x}''_-(0)$  direction.

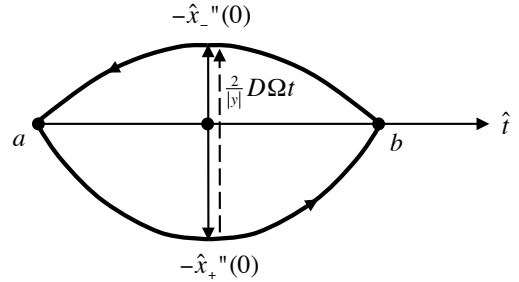


FIG. 3: Depiction of forward and backward loops in the two-dimensional case.

$C_-$  in the plane of  $\hat{\mathbf{t}}$  and  $\mathbf{x}''_-(0)$  as shown in Figure 1. Now take two endpoints  $\mathbf{a}$  and  $\mathbf{b}$  close to  $\mathbf{X}$ , and take  $\hat{\mathbf{t}}$  to be parallel to  $\mathbf{b} - \mathbf{a}$ . By small translations of the parabolas in Figure 1 in the  $-\mathbf{x}''_+(0)$  and  $-\mathbf{x}''_-(0)$  directions, we can asymptotically construct the forward plus backward loop with these endpoints. Pictorially, the difference  $\mathbf{x}''_+(0) - \mathbf{x}''_-(0)$  corresponds to the “openness” of the constructed fluctuation loop as shown in Figure 2. The dashed vector marks the displacement between the turning points of the  $\mathbf{a}$  to  $\mathbf{b}$  and  $\mathbf{b}$  to  $\mathbf{a}$  parabolas; it is proportional to  $[\mathbf{x}''(0)] = \frac{2}{|\mathbf{u}|} D\Omega\hat{\mathbf{t}}$ .

In two dimensions, we can develop further intuition. In that case, the vorticity tensor takes the form

$$\Omega = \begin{bmatrix} 0 & -\omega \\ \omega & 0 \end{bmatrix}, \quad (30)$$

where  $\omega := \partial_1(D^{-1}\mathbf{u})_2 - \partial_2(D^{-1}\mathbf{u})_1$ , is the *scalar vorticity*. For  $\omega > 0$ , (27) is the generator of a counterclockwise rotation. Figure 3 is the two dimensional version of Figure 2, drawn assuming scalar diffusion ( $D$  proportional to the identity) and  $\omega > 0$ . The counterclockwise circulation around the loop agrees with the counterclockwise rotation associated with the vorticity. This is the choice you would make to reduce “headwinds” and thereby reduce the stochastic action.

#### IV. VORTICITY-INDUCED BIFURCATIONS

The global effects of vorticity-induced bending of rays are most simply displayed in a class of two-dimensional examples we call *pure shear*: we have isotropic diffusion  $D = I$ , and the flows  $\mathbf{u}$  on  $\mathbb{R}^2$  are

$$\mathbf{u} = u(y)\hat{\mathbf{y}}, \quad (31)$$

where the *velocity profile*  $u(y)$  is a given positive function. The  $x$ -component of the ray ODE (27) is

$$\frac{d}{ds}\left(u\frac{dx}{ds}\right) = u'(y)\frac{dy}{ds}, \quad (32)$$

which has the first integral

$$u(y)\left(1 - \frac{dx}{ds}\right) = \sigma = \text{constant}. \quad (33)$$

(33) is analogous to Snell's law in optics: that is,  $\frac{dx}{ds} = \cos\theta$ , where  $\theta$  is the local angle of the ray with respect to  $\hat{\mathbf{x}}$ . Hence, (33) implies that  $\theta$  changes with elevation  $y$  due to gradients of the velocity profile  $u(y)$ . In this sense, we have "refraction by shear." Due to the first integral (33), the geometric action of a ray  $C$  has the simple expression

$$S = \int_C u ds - u dx = \int_C u\left(1 - \frac{dx}{ds}\right) ds = \sigma L, \quad (34)$$

where  $L$  is the arclength of  $C$ . Deterministic paths are immediately recognized from the effective Snell's law (33) and (34): The geometric action vanishes if the constant  $\sigma$  is zero, and then  $\frac{dx}{ds} \equiv 1$ , which corresponds to horizontal straight lines oriented to the right. These lines are the obvious integral curves of the shear flow.

Next, we examine rays that undergo a net displacement in the negative  $x$ -direction, which is "against the wind." By the mean value theorem, such a ray must have a *turning point*  $\mathbf{x}_*$ , where  $\frac{dx}{ds} = -1$ . Evaluating (33) at the turning point, we have  $\sigma = 2u_* := 2u(y_*)$ , where  $y_*$  is the elevation of the turning point. Hence, (33) can be written as

$$u\frac{dx}{ds} = u - 2u_*, \quad (35)$$

and the geometric action becomes

$$S = 2u_*L. \quad (36)$$

We can determine a governing equation for the vertical component  $y(s)$  of  $\mathbf{x}(s)$ , by evoking the geometric identity  $\left(\frac{dx}{ds}\right)^2 + \left(\frac{dy}{ds}\right)^2 = 1$ , and using the effective Snell's law (35):

$$u^2\left(\frac{dy}{ds}\right)^2 = 4u_*(u(y) - u_*). \quad (37)$$

Since  $u(y)$  is the deterministic speed along the ray, we recognize  $u\frac{d}{ds}$  as the time derivative  $\frac{d}{dt}$ , and we write (35) and (37) respectively as

$$\dot{x} = u(y) - 2u_*, \quad (38)$$

$$\dot{y}^2 = 4u_*(u(y) - u_*). \quad (39)$$

The second equation is the first integral of the second order differential equation

$$\ddot{y} = 4u_*u'(y). \quad (40)$$

Here,  $-u'(y)$  is the scalar vorticity of the shear flow, so (40) directly expresses "bending by vorticity."

We can construct rays explicitly for the instructive case of quadratic shear flow, with

$$u(y) = \frac{1}{2}(y^2 + \epsilon^2), \quad (41)$$

where  $\epsilon$  is a positive parameter. The minimum positive  $x$ -velocity happens along the  $x$ -axis. We expect that rays with a start to finish displacement in the negative  $x$ -direction bend toward the  $x$ -axis, to take advantage of the reduced headwind there. Such a ray must have a turning point. By the  $x$  and  $t$  translation invariance of (38) and (39), we can use the turning point to mark the origins of  $x$  and  $t$ , so we have initial conditions  $x(0) = 0, y(0) = y_*, \dot{y}(0) = 0$ . The solutions of (38), (39) with these initial conditions are

$$y = y(t, y_*) = y_* \cosh \tau, \quad (42)$$

$$x = x(t, y_*) = \frac{y_*^2}{4\sqrt{y_*^2 + \epsilon^2}}(\cosh \tau \sinh \tau - \tau) - \frac{\sqrt{y_*^2 + \epsilon^2}}{2}\tau. \quad (43)$$

Here,  $\tau$  is the scaled time

$$\tau := \sqrt{y_*^2 + \epsilon^2}t. \quad (44)$$

For each value of  $y_*$  we obtain a corresponding ray represented by a parametric curve

$$\mathbf{x}(t) = x(t, y_*)\hat{\mathbf{x}} + y(t, y_*)\hat{\mathbf{y}}. \quad (45)$$

We present a pictorial narrative of these rays for the case  $\epsilon = 0.3$ , and this shows how segments of rays produce net displacements in the negative  $x$ -direction. Figure 4 shows the ray with turning point elevation  $y_* = 1$ . The most striking feature is the teardrop-shaped loop with counterclockwise orientation. The "teardrop" persists for all  $y_* > 0$ . From (38), we see that the vertical tangents happen at the elevation  $y$  for which the shear velocity  $u(y)$  is twice as high as at the elevation of the turning point. As  $y_* \rightarrow 0$ , the bottom of the teardrop between the vertical tangents flattens out into a long, left-oriented segment close to the  $x$ -axis. We see this in Figure 5, which depicts the ray with  $y_* = .01$ .

A ray which interpolates between given starting and ending points  $\mathbf{a}$  and  $\mathbf{b}$  is called a *connector*. We examine the connectors with

$$\mathbf{a} = \frac{l}{2}\hat{\mathbf{x}} + \hat{\mathbf{y}}, \mathbf{b} = -\frac{l}{2}\hat{\mathbf{x}} + \hat{\mathbf{y}}, \quad (46)$$

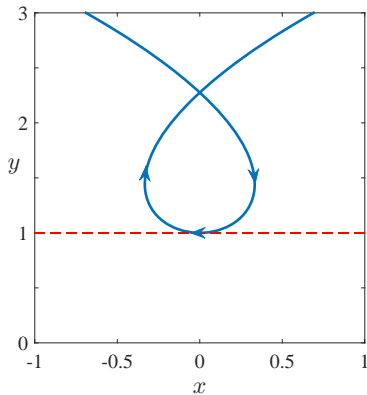


FIG. 4: Transition path ray for the case  $y_* = 1$  and  $\epsilon = 0.3$ .

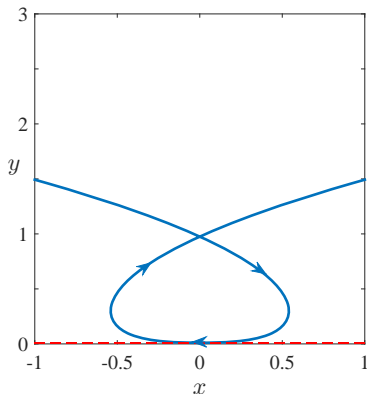


FIG. 5: Transition path ray for the case  $y_* = 0.01$  and  $\epsilon = 0.3$ .

which makes a net displacement of length  $l$  in the negative  $x$ -direction. These connectors are segments of the “teardrop,” symmetric about the  $x$ -axis. Given  $l$ , there are discrete choices for the turning point elevations  $y_*$  of possible connectors. Let  $\tau = \tau_b > 0$  be the value of scaled time marking the ending point **b**. By symmetry,  $\tau = -\tau_b$  marks the starting point **a**, and the connector passes through the turning point  $y_*\hat{y}$  at  $\tau = 0$ . At  $\tau = \tau_b$ , the elevation  $y$  is unity, so (42) implies

$$y_* \cosh \tau_b = 1. \quad (47)$$

Given  $0 < y_* < 1$ , we solve for  $\tau_b$ ,

$$\tau_b = \log \frac{1 + \sqrt{1 - y_*^2}}{y_*}. \quad (48)$$

The actual time of flight from **a** to **b** is

$$T = \frac{2\tau_b}{\sqrt{y_*^2 + \epsilon^2}} + \frac{2}{\sqrt{y_*^2 + \epsilon^2}} \log \frac{1 + \sqrt{1 - y_*^2}}{y_*} \quad (49)$$

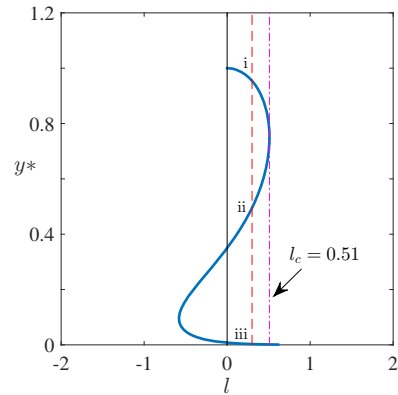


FIG. 6: Plot of Equation (53) showing the allowed values of  $y_*$  as a function of  $l$  and  $\epsilon = 0.3$ . The turning point at  $l_c$  corresponds to a saddle-node bifurcation in which two transition paths with endpoints **a** and **b** collide and annihilate.

At  $\tau = -\tau_b$ ,  $x = \frac{l}{2}$ , and then (43) implies

$$\frac{l}{2} = \frac{y_*^2}{4\sqrt{y_*^2 + \epsilon^2}} (\tau_b - \cosh \tau_b \sinh \tau_b) + \frac{\sqrt{y_*^2 + \epsilon^2}}{2} \tau_b. \quad (50)$$

Substituting for  $\tau_b$  from (48), this reduces to

$$l = \left( \sqrt{y_*^2 + \epsilon^2} + \frac{y_*^2}{2\sqrt{y_*^2 + \epsilon^2}} \right) \log \left[ \frac{1 + \sqrt{1 - y_*^2}}{y_*} \right] - \frac{\sqrt{1 - y_*^2}}{2\sqrt{y_*^2 + \epsilon^2}}. \quad (51)$$

The graph of  $y_*$  vs  $l$  in Figure 6 based on (51) is plotted with  $\epsilon = 0.3$ , but is qualitatively correct for  $0 < \epsilon \ll 1$ . For connectors with a net displacement in the negative  $x$ -direction, the relevant portion of this graph has  $l > 0$ , marked by the solid curves. There are three branches of roots for  $y_*$  as functions of  $l$ , which we’ve labeled i, ii, and iii. Branches i and ii coalesce in a saddle-node bifurcation as  $l \rightarrow l_c \simeq 0.51$ . Furthermore, the branches i and ii have definite limits as  $\epsilon \rightarrow 0$ , and the saddle-node bifurcation survives with  $l_c \rightarrow 0.4852$ . Figure 7 depicts the connecting pathways corresponding to branches i, ii and iii for  $\epsilon = 0.3$ .

Which connector has the smallest geometric action? We can compute the arclength  $L$  of connectors, and then their geometric actions from  $S = 2u_*L$  as in (36). Since  $u = u(y)$  is the speed along a ray, the arclength of a connector  $C$  is

$$L = \int_C u dt = \int_C (\dot{x} + 2u_*) dt = -l + 2u_*T. \quad (52)$$

Substituting into (42) the time of flight  $T$  from (49), and  $l$  from (51), we obtain for the action

$$S = \frac{\sqrt{y_*^2 + \epsilon^2}}{2} \left( (y_*^2 + 2\epsilon^2) \log \frac{1 + \sqrt{1 - y_*^2}}{y_*} + \sqrt{1 - y_*^2} \right). \quad (53)$$

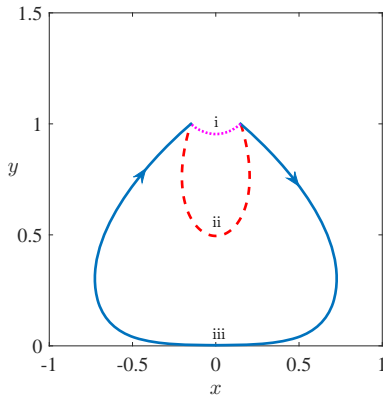


FIG. 7: Plot of the three connector solutions corresponding to the three branches of Figure 6 for  $l = 0.3$  and  $\epsilon = 0.3$ .

From (53), we find that the shorter branch i connector has the smallest geometric action. Apparently, the branch ii connector is a stationary point of geometric action, but not a minimum.

Branch iii in Figure 7 and its corresponding connector persist for all  $l > 0$ . In the limit  $\epsilon \rightarrow 0$ , branch iii of the  $y_*$  vs  $l$  relation is asymptotic to

$$y_* \sim 2 \exp \left[ -\frac{1}{2\epsilon^2} - \frac{l}{\epsilon} \right]. \quad (54)$$

Figure 7 depicts the branch iii connector for  $\epsilon = 0.3$ . The branch iii connector has a singular structure as  $\epsilon \rightarrow 0$ . In particular, its arclength diverges like

$$L \sim \frac{1}{\epsilon} + l. \quad (55)$$

Its geometric action is asymptotic to

$$S \sim \epsilon. \quad (56)$$

In the limit  $\epsilon \rightarrow 0$  with  $l$  fixed, we see that the branch iii connector is the most probable path, beating out connector i, for  $0 < l < l_c$ . The “strategy” of connector iii

is clear: Descend from  $y = 1$  to the  $x$ -axis, stay close to the  $x$ -axis for a long time, and finally ascend back up to  $y = 1$ . In this way, the resistance against the deterministic flow is minimized. The descent and ascent branches have little cost, because they are almost parallel to the deterministic flow. Most of the leftwards motion happens along the segment close to the  $x$ -axis, where the headwind is small.

We expect that as we close the gap between **a** and **b** by decreasing  $l$ , we’ll eventually find  $l = l_*$  so that the branch i connector becomes the most probable path for  $0 < l < l_*$ . By an elementary calculation, we find  $l_* \sim \epsilon$  as  $\epsilon \rightarrow 0$ .

## V. CONCLUSIONS AND FUTURE DIRECTIONS

The breaking of detailed balance is “made visible” by the splitting of forward and backward most probable paths between two fixed endpoints. This is a first hint that detailed balance and its breaking can be inferred directly from recorded histories of a stochastic dynamical system, in a suitable space of observables. A first “obvious” proposal, while achievable in principle, may often be difficult to implement in practice: this involves collecting records of trajectories that connect two small regions around given endpoints, and observing directly the aforementioned splitting between forward and backward paths. At small noise levels, there are long waits to collect these trajectories, and then you might want to have many of them for averaging. It would be much better if detailed balance or its breaking can be detected by some simple processing of data from a few, or even one trajectory. Such a procedure in fact exists. It has been fully developed by the authors for linear stochastic dynamical systems, and numerically tested for a simple circuit example [15]. More recently, we’ve found that its nonlinear generalization is straightforward and that story will get its own paper [18].

## VI. ACKNOWLEDGEMENT

We gratefully acknowledge the assistance of Varun Gupta with the preparation of Figures 1, 2, and 3.

- 
- [1] R. P. Feynman, A. R. Hibbs, *Quantum Mechanics and Path Integrals* (McGraw-Hill, New York, 1965).
  - [2] A. D. Ventsel, M. I. Freidlin, *Russian Mathematical Surveys* **1**, 1 (1970).
  - [3] M. I. Freidlin, A. D. Wentzell, *Random Perturbations of Dynamical Systems*. A Series of Comprehensive Studies in Mathematics (Springer, 2012).
  - [4] N. Berglund, B. Gentz, *Noise-Induced Phenomena in Slow-Fast Dynamical Systems: A Sample-Paths Approach*. Probability and Its Applications (Springer, 2006).
  - [5] A. Prados, P. I. Lasanta, P. I. Hurtado, *Phys. Rev. Lett.* **107**, 140601 (2011).
  - [6] L. Bertini, A. De Sole, D. Gabrielli, G. Jona-Lasinio, C. Landim, *Rev. Mod. Phys.* **87**, 593 (2015).
  - [7] R. S. Maier, D. L. Stein, *SIAM J. Appl. Math.* **57**, 752 (1997).
  - [8] D. G. Luchinsky, P. V. E. McClintock, M. I. Dykman, *Rep. Prog. Phys.* **61**, 905 (1998).
  - [9] M. Heymann, E. Vanden-Eijnden, *Phys. Rev. Lett.* **100**, 140601 (2008).

- [10] M. Heymann, E. Vanden-Eijnden, *Commun. Pure Appl. Math.* **61**, 1052 (2008).
- [11] M. Heymann, *Minimum Action Curves in Degenerate Finsler Metrics, Lecture Notes in Mathematics*, vol. 2134 (Springer, 2015).
- [12] R. S. Maier, D. L. Stein, *Phys. Rev. Lett.* **71**, 1783 (1993).
- [13] R. K. P. Zia, B. Schmittmann, *J. Stat. Mech.-Theory and Experiment* P07012 (2007).
- [14] P. H. Dannenberg, J. C. Neu, S. W. Teitsworth, *Phys. Rev. Lett.* **113**, 020601 (2014).
- [15] A. Ghanta, J. C. Neu, S. W. Teitsworth, *Phys. Rev. E* **95**, 032128 (2017).
- [16] M. I. Dykman, E. Mori, J. Ross, P. M. Hunt, *J. Chem. Phys.* **100**, 5735 (1994).
- [17] M. Born, E. Wolf, *Principles of Optics*, 6th edition (1980).
- [18] J. C. Neu, S. W. Teitsworth, unpublished (2017).